

# Impact Depth and the Interaction with Impact Speed Affect the Severity of Contusion Spinal Cord Injury in Rats

Cameron J. Lam,<sup>1,2</sup> Peggy Assinck,<sup>2,3</sup> Jie Liu,<sup>2</sup> Wolfram Tetzlaff,<sup>2,4</sup> and Thomas R. Oxland<sup>1,2</sup>

## Abstract

Spinal cord injury (SCI) biomechanics suggest that the mechanical factors of impact depth and speed affect the severity of contusion injury, but their interaction is not well understood. The primary aim of this work was to examine both the individual and combined effects of impact depth and speed in contusion SCI on the cervical spinal cord. Spinal cord contusions between C5 and C6 were produced in anesthetized rats at impact speeds of 8, 80, or 800 mm/s with displacements of 0.9 or 1.5 mm ( $n=8/\text{group}$ ). After 7 days postinjury, rats were assessed for open-field behavior, euthanized, and spinal cords were harvested. Spinal cord tissue sections were stained for demyelination (myelin-based protein) and tissue sparing (Luxol fast blue). In parallel, a finite element model of rat spinal cord was used to examine the resulting maximum principal strain in the spinal cord during impact. Increasing impact depth from 0.9 to 1.5 mm reduced open-field scores ( $p<0.01$ ) above 80 mm/s, reduced gray (GM) and white matter (WM) sparing ( $p<0.01$ ), and increased the amount of demyelination ( $p<0.01$ ). Increasing impact speed showed similar results at the 1.5-mm impact depth, but not the 0.9-mm impact depth. Linear correlation analysis with finite element analysis strain showed correlations ( $p<0.001$ ) with nerve fiber damage in the ventral ( $R^2=0.86$ ) and lateral ( $R^2=0.74$ ) regions of the spinal cord and with WM ( $R^2=0.90$ ) and GM ( $R^2=0.76$ ) sparing. The results demonstrate that impact depth is more important in determining the severity of SCI and that threshold interactions exist between impact depth and speed.

**Key words:** behavior; cervical; contusion; finite element analysis; impact depth; impact speed; spinal cord injury; strain

## Introduction

**T**RAUMATIC SPINAL CORD INJURY (SCI) occurs when the spinal column experiences structural failure and is most commonly caused by motor vehicle collisions, falls, sports-related accidents, work-related accidents, and violence.<sup>1–3</sup> These injuries often result in long-term disability and have incidence rates estimated at 1785 per year in Canada and 12,000 per year in the United States.<sup>3,4</sup> As a result, these injuries create health care costs of an average of \$1.1–\$3.5 million (U.S. dollars) over the lifetime of an individual, not including the costs associated with loss of quality of life and productivity.<sup>5</sup>

Much current research has focused on the understanding of the mechanism of SCI and the resulting effects. Failure of the spinal column can cause a variety of different mechanisms of primary injury. Clinically, burst fractures make up one of the most common types of SCI, at approximately 30% of all SCI.<sup>1,2</sup> These types of injuries result from compression of the vertebral bodies causing the spinal column to fracture and impinge on the spinal cord, resulting

in an injury mechanism known as a contusion. Various contusion models have been developed to mimic the injury under specific experimental conditions (0.86–1.94 mm and 80–540 mm/s),<sup>6</sup> but most do not offer independent control and decoupling of both impact depth and speed.<sup>6–8</sup> One of the most common injury models, where an impactor of known weight follows a guided release at a given height, couples both the impact depth and speed together. Increasing the drop height of the impactor increases the impact speed because it is given more time to accelerate, but will also increase the amount of energy available to impact the cord resulting in an increase in the force and depth of injury.

Independently, it has been shown that the severity of SCI is dependent on the impact depth and speed of the injury. Experimental studies have shown that increasing impact speed results in greater disruption of the white matter (WM; 3–300 mm/s at 1-mm impact depth) and damage to the blood–spinal cord barrier (489, 690, and 974 mm/s at 1.65-, 2.14-, and 2.88-mm impact depths, respectively).<sup>9,10</sup> Additionally, studies have also shown that increasing impact depth in contusion injuries (0.8–1.1 mm) resulted

<sup>1</sup>Orthopedic and Injury Biomechanics Lab, Departments of Mechanical Engineering and Orthopedics, <sup>3</sup>Graduate Program in Neuroscience, <sup>4</sup>Department of Zoology and Department of Surgery, University of British Columbia, Vancouver, British Columbia, Canada.

<sup>2</sup>International Collaboration on Repair Discoveries (ICORD), Blusson Spinal Cord Center, Vancouver, British Columbia, Canada.

in larger spinal cord lesions and larger areas of demyelination,<sup>11–14</sup> as well as the existence of tissue-level strain thresholds for axonal injury.<sup>15,16</sup>

SCI is characterized by an initial primary (immediate) injury causing cell death and a lesion around the injury site. Over the next few days to weeks, a cascade of biological responses causes formation of a glial scar around the injury site, which creates secondary injuries and further degeneration.<sup>2,17</sup> Many of the cells that are lost in the WM are oligodendrocytes and result in the demyelination of nearby axons. This demyelination in the spinal cord has been suggested to contribute to physiological impairment.<sup>18–21</sup> Contusion injuries have shown more-severe and extensive demyelination than transection injuries, and the lesion spans a much larger area.<sup>22</sup>

The variation of injury speed and impact depth in contusion injuries has been thought to lead to differences in injury morphology. This study examines these mechanical effects independently and interactively in the rat model in an attempt to describe relative importance of these parameters in determining injury severity. It has also been reported that, in the rat dislocation injury model, the magnitude of dislocation significantly affected the severity of injury, but that the speed of dislocation had no effect.<sup>23</sup> The motivation of this study is to combine both the experimental and computational work to attempt to understand how mechanical injury factors result in a range of functional outcomes, biological response in the spinal cord, and mechanical strain patterns in the spinal cord after secondary injury.

## Methods

### Contusion injury

All experimental procedures were performed under a protocol approved by the University of British Columbia's Office of Research Services Animal Care Committee (Vancouver, BC, Canada) in accord with the guidelines published by the Canadian Council on Animal Care. Forty-eight male Sprague-Dawley rats (~300 g) were separated equally into six different injury groups and one surgical sham group (Table 1). Sham animals received the same surgical procedure and touch force from the impactor, but did not receive an injury. Each injury group received a maximum impact speed of 8, 80, or 800 mm/s to a maximum impact depth of either 0.9 or 1.5 mm. The speed and impact depth parameters were chosen to obtain a wide range of injury severities and enable the investigation of the depth-velocity interaction. Animals were exposed to the facilities 1 week before injury and individually handled for 15 min daily to familiarize them with human interaction to reduce stress both before and postinjury.

Upon arrival to our vivarium, animals were allowed to explore the open field for 4 min to acclimatize them before any baseline behavioral assessment. To obtain baseline behavioral assessment, each rat was placed in an open field for 4 min and scored by two independent researchers using a modified open-field cervical SCI scale.<sup>24</sup> This also served as an additional way for the animals to

familiarize themselves with the open field before injury. Once baseline behavior was obtained, rats were deeply anesthetized with aerosolized isoflurane (induction, 5%; maintenance, 2%; Baxter Co., Mississauga, ON, Canada). Subcutaneous (s.c.) injection of buprenorphine (0.03 mg/kg) was given to mitigate any possibility of acute pain. After anesthetization to a surgical plane, the spinal column was exposed dorsally from the second to the seventh cervical vertebrae (C2–C7). A laminectomy was performed between the fifth and sixth cervical vertebrae (C5–C6) to expose the spinal cord and dura. Custom stainless-steel vertebral clamps were attached rigidly to hold both the C5 and C6 vertebrae in place. The custom contusion injury device and stereotaxic frame, as well as vertebral clamps used in this study, were designed by Choo and colleagues and first described in 2007.<sup>25</sup> This device consists of an electromagnetic actuator, impactor tip, stereotaxic frame, and sensors used to measure force, displacement, and acceleration (Fig. 1). Sensors were limited to sampling the data at 4000 Hz. Once the clamps were attached to the contusion device, the 2-mm diameter impactor head was lowered in 50- $\mu$ m increments until a touch force of 0.03 N was reached, dimpling the surface of the dura to achieve a consistent datum for all injuries.<sup>26</sup> The impactor was then retracted 6 mm above the dura before accelerating downward to impact the cord using the predetermined depth and speed. Immediately after injury, the impactor was retracted 6 mm above the starting point with no dwell time.

After contusion injury, the vertebral clamps were removed and the skin and muscle were sutured to promote healing and avoid infection. Animals were monitored four times daily and given s.c. buprenorphine (0.03 mg/kg) three times daily for 3 days. After the 7-day survival period, each animal was reassessed in the open-field behavioral test before sacrifice with an overdose of chloral hydrate (0.5 g/kg, intraperitoneally; Sigma-Aldrich Co., St. Louis, MO). All animals then were perfused with an intracardial needle with 250 mL of phosphate-buffered saline (PBS) and followed with 500 mL of 4% paraformaldehyde (PFA) in order to fix the tissue. The spinal cord was dissected from the animal approximately  $\pm$  5 mm rostral and caudal around the injury epicenter and fixed overnight in 4% PFA. Each cord was cryoprotected in increasing concentrations of sucrose solutions (12%, 18%, and 24%) for 12 h at each grade and frozen in optimum cutting temperature compound using isopentane and dry ice before being cryosectioned in 20- $\mu$ m increments in the transverse plane (cross-sectional) in serial sets.

### Open-field behavioral analysis

The more sensitive open-field evaluation tool developed by Martinez and colleagues was modified for mid-line injuries by including a bilateral assessment of individual limb score and used for this study.<sup>24</sup> Animals were placed in the open field (120  $\times$  150 cm) for a period of 4 min, and their forelimb movement, weight support, paw stepping, digit position, running coordination, and tail position were evaluated and scored as described in detail below. If the animal did not move for a period of 20 sec or longer, it was picked up and placed at the center of the open field. Two examiners, blinded to the injury each animal received, scored the behavior for each animal by consulting with each other to complete each category. All categories were scored separately with a maximum total score of 72. In addition to scoring the fore- and hindlimbs separately, both the left- and right-side limbs were scored individually.

### Luxol fast blue imaging and analysis

After serial sectioning of the spinal cord tissue, one set of slides was stained with Luxol fast blue (LFB) for WM and GM tissue sparing analysis. Slides were thawed and dipped into a 1% LFB solution overnight at 60°C and differentiated in lithium carbonate the following day. All images were captured on an AxioPlan2 microscope (Carl Zeiss, Thornwood, NY) using a 2.5 $\times$  objective.

TABLE 1. EXPERIMENTAL IMPACT INJURY CONDITIONS

Injury group	Displacement (mm)	Speed (mm/s)	No. of rats
1	0.9	8	8
2	0.9	80	7
3	0.9	800	8
4	1.5	8	6
5	1.5	80	7
6	1.5	800	7
7	Surgical sham	Surgical sham	5

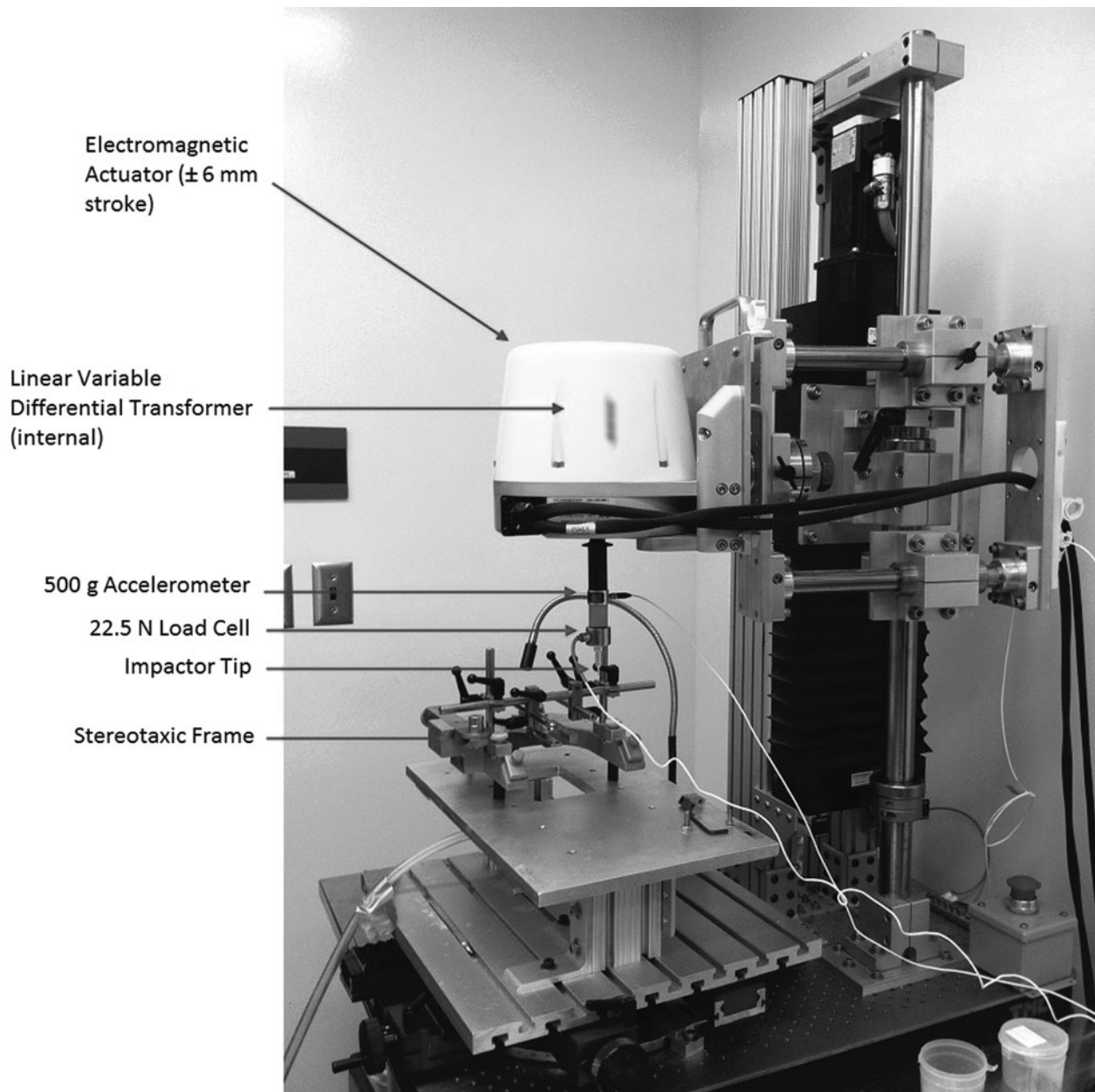


**FIG. 1.** Photograph of the custom-designed UBC multi-mechanism injury system. The speed and depth of the impactor is computer controlled through the electromagnetic actuator. The linear variable differential transformer, accelerometer, and load cell record the biomechanical data.

Images were captured through the attached monochrome camera (Retiga Exi; QImaging, Burnaby, BC, Canada) using Northern Eclipse acquisition software (Empix Imaging, Mississauga, ON, Canada). Each set of serial images was stitched together using Adobe Photoshop CS3 (v10.0) using the photomerge function to represent the entire section. The injury epicenter was defined as the section containing the largest lesion area. Images were captured with 1-mm spacing between each section from 3 mm rostral to 3 mm caudal of the injury epicenter.

Each cross-sectional image was segregated into damaged WM, damaged GM, intact WM, and intact GM regions in Photoshop using the magic wand tool to select areas of similar pixel intensity. In some sections, the tissue was so damaged that an estimation of the GM and WM boundary was hand drawn based on nondamaged tissue in the sham spinal cords. After being sectioned into these four

regions, each image was converted to an 8-bit image and measured for total area using a constant threshold of 215/255 using ImageJ (v1.47c; National Institutes of Health, Bethesda, MD). Total percentage of GM spared and total percentage of WM spared were recorded as the measured areas normalized to the total area of GM or WM in the section being analyzed identified by the LFB stain.<sup>27</sup> Sectioning using the magic wand tool, allowing the user to select pixels based on tone and color as opposed to a defined shape, was compared to completely manual sectioning and found to only have a root mean square difference of 6.5%.

#### *Immunohistochemistry imaging and analysis*

A second set of slides was immunostained with chicken anti-myelin-based protein (MBP), mouse anti-neurofilament-200

(NF-200), and mouse anti-beta III tubulin to detect demyelination of axons surrounding the injury epicenter in the subsequent analysis. All slides were thawed from frozen at room temperature for 30 min before rehydrating for 10 min in 0.01 M of PBS, then delipidized in increasing and decreasing concentrations of ethanol (50%, 70%, 90%, 95%, 100%, 95%, 90%, 70%, and 50%). The tissue was washed in 0.01 M of PBS before being blocked for 30 min in 10% normal donkey serum before overnight incubation at room temperature in the primary antibody (Ab) dilution (1:200 chicken anti-MBP; Aves Labs Inc., Tigard, OR; 1:500 mouse anti-NF-200; Sigma-Aldrich; 1:500 mouse anti-beta III tubulin; Sigma-Aldrich; and 1:1000 rabbit anti-glial fibrillary acidic protein; Dako Canada Inc., Burlington, ON, Canada) in 0.01 M of PBS containing 0.1% Triton X-100. After incubation, slides were washed for 5 min in 0.01 M of PBS three times and incubated in the secondary Ab dilution (1:200 Alexa Fluor 594 donkey anti-mouse, 1:200 Alexa Fluor 488 donkey anti-chicken, and 1:200 Alexa Fluor 405 donkey anti-rabbit; Jackson ImmunoResearch Laboratories, West Grove, PA) for 2 h in a light opaque container. Sections were then washed for 5 min in 0.01 M of PBS and mounted in Fluoromount-G (Southern Biotechnology, Birmingham, AL), to help prevent photobleaching, and covered with glass cover-slips (No. 1.5; VWR, Radnor, PA).

All images were acquired using a Zeiss microscope (Axio Observer Z1; Carl Zeiss) with a 40 $\times$  objective and equipped with a Yokogawa spinning disc confocal device (CSU-X1; Yokogawa Corporation of America, Sugar Land, TX) and a motorized scanning stage (MS-2000; Applied Scientific Instrumentation, Eugene, OR). Exposure settings for image capture were automatically optimized through the Zen software (Blue v1.0.1.0; Carl Zeiss Microscopy GmbH, Jena, Germany) for each section because pixel intensity or area was not a factor in identifying the final outcome measure. The injury epicenter was defined as the section with the largest lesion area. Sections were imaged with a spacing of 1 mm from 3 mm rostral to 3 mm caudal around the injury epicenter. Systematic random sampling through the cross-sectional images through the ventral and lateral white funiculi regions was used to image the WM. The lateral funiculi region was determined as all WM lateral to a line drawn in the anterior-posterior direction connected to the outermost edge of the lateral horn. The ventral funiculi region was captured as all WM located between the anterior median fissure and the medial edge of the anterior horn.

A 75 $\times$ 75  $\mu$ m grid was overlaid on top of the image, and sampling frames were selected at every fourth 75 $\times$ 75  $\mu$ m square until the entire region of interest (ROI) was sampled. Images were not sampled at the edge of the tissue or on the GM and WM border. Within each 75 $\times$ 75  $\mu$ m square, a smaller, 25 $\times$ 25  $\mu$ m, ROI at the center was used to identify and count all demyelinated, swollen, and pathological axons (Fig. 2). A demyelinated axon was classified if most of its myelin sheath was missing, whereas pathological

axons were defined as axons that were no longer tightly wrapped by myelin. All demyelinated, swollen, and pathological axons were considered damaged nerve fibers used to calculate the percentage of damaged nerve fibers in the tissue region.

### Computational model

A finite element model of the rat cervical spine developed by Russell and colleagues was used to compute the maximum principal strain in specific regions of the cord during a contusion injury.<sup>28</sup> Hexahedral three-dimensional elements were used for the GM, WM, and dura mater while tetrahedral elements were used for the vertebrae and intervertebral discs. A total of 235,734 three-dimensional elements made up the C3–C6 segment of the spine, and 18,972 smooth particles were created to mimic the cerebrospinal fluid (CSF) surrounding the cord. For this study, the impactor speed during the survival study was used as input to the finite element analysis (FEA) to control the speed and depth of the impactor tip for each injury group. Loading and boundary conditions for contusion injuries were modeled to replicate the experimental setup. All vertebrae and intervertebral discs were created as rigid bodies, and the clamped vertebrae around the injury epicenter were fixed in PAM-CRASH (Version 7.5; ESI Group, Paris, France). The rostral and caudal ends of the dura were constrained thoroughly, preventing motion along the axis of the cord. Specific ROIs quantified by Choo and colleagues and Russell and colleagues were modified and outlined in the model to reflect the dorsal, lateral, and ventral regions of the WM and GM.<sup>28,29</sup> Each cross-section was spaced at 1-mm increments rostral-caudally from the injury epicenter. Maximum principal strain was recorded in each of these regions during contusion simulation for comparison with the demyelination, tissue sparing, and behavioral deficit recorded experimentally.

### Statistical analysis

For the open-field behavioral results, the scores were compared using a nonparametric Kruskal-Wallis' analysis of variance (ANOVA) comparison of ranks for statistical significance. Any scores that displayed a *p* value of less than 0.05 were further evaluated using multiple comparisons of mean ranks. A total of 16 individual group comparisons, between groups with similar impact depth, impact speed, and impact energy were done with Mann-Whitney's U test using a Bonferroni's correction, bringing the corrected alpha value to  $\frac{0.05}{6} = 0.00833$ .

For the LFB and MBP tissue analysis, normal distribution was determined using Shapiro-Wilk's test. Both the arcsine transformation of tissue sparing and percentage of damaged nerve fibers were normally distributed. A two-way ANOVA test was carried out to compare the effects of impact speed and impact depth on demyelination as an indicator of secondary injury. An alpha level of 0.05 was used for the ANOVA and a post-hoc unequal N Tukey's test followed if significance was found.

For the normally distributed data sets, a linear correlation analysis was employed to identify the strength of the relationship between the tissue sparing and percentage of damaged nerve fibers with the mechanical impact factors and the regional maximum principal strains. Correlation coefficient values were recorded for all comparisons and were reported along with complete scatterplot graphs to visualize the data pool. Nonparametric Spearman's rank-order tests were used to determine the correlations between the open-field scores with impact speed and depth, as well as maximum principal strain.

## Results

### Contusion impact mechanics

Contusion SCI was induced in 48 male Sprague-Dawley rats with 5 surgical shams. Some animals experienced complications

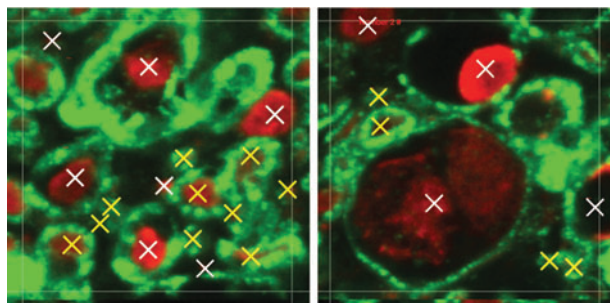


**FIG. 2.** Shown is a 25 $\times$ 25  $\mu$ m axon counting region of interest. Examples of healthy nerve fibres (yellow) and damaged nerve fibres (white) are shown. Color image is available online at [www.liebertpub.com/neu](http://www.liebertpub.com/neu)

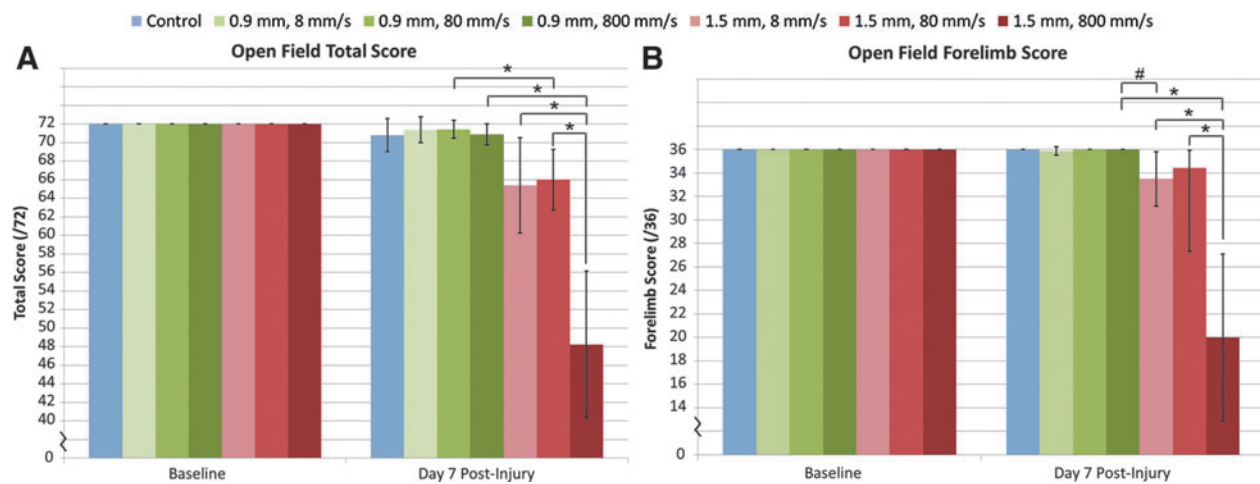


**FIG. 3.** Open-field behavioral results. (A) After injury, a significant reduction in total score was observed when impact depth was increased from 0.9 to 1.5 mm above 80 mm/s impact velocity (\* $p < 0.0030125$ ). (B) Analysis of forelimb scores showed a large reduction in score between the two groups with similar applied impact energy and different impact depths (# $p = 0.003743$ ). Data shown are mean  $\pm$  standard deviation. Color image is available online at [www.liebertpub.com/neu](http://www.liebertpub.com/neu)

during the surgical laminectomy or in the 7-day survival period and were euthanized, resulting in fewer animals in those groups (see Table 1). Impact depth was set to 0.9 and 1.5 mm and saw little relative variation with a standard deviation (SD) of depth less than 0.3% of the average. Impact speeds of 8, 80, and 800 mm/s were set in the software. The 8-mm/s impacts showed SD of approximately 12% of the average speed, whereas both the 80- and 800-mm/s impacts had an SD of less than 2% of the average (Table 2). Given the increase in magnitude between impact speed groups, the absolute variation of the slow impact group was deemed acceptable.

No significant difference in energy applied to the spinal cord ( $p > 0.05$ ) was observed between groups 1 and 2, 2 and 3, and 3 and 4 (Table 2). The energy applied to the spinal cord in the 0.9 mm–800 mm/s and 1.5 mm–8.0 mm/s groups fell within a similar range.

**Behavioral analysis**

Scores were compiled as a hindlimb score (of 36), forelimb score (of 36), and a combined total score (of 72). All animals received a score of 72 at baseline assessment. At 7 days postinjury, animals that received a 1.5-mm depth injury saw a significant reduction in hindlimb, forelimb, and total score ( $p < 0.007$ ), which was not shown by the 0.9-mm-depth injury regardless of impact speed. Postinjury group comparison showed a significant reduction of total score ( $p < 0.003125$ ) when impact depth was increased from 0.9 to 1.5 mm above an 80-mm/s impact. Increased impact speed to 800 mm/s also displayed a significant ( $p < 0.003125$ ) reduction of

total score in the open field at the 1.5-mm impact depth (Fig. 3A). Injury groups that had a similar range of impact energy displayed no change in total score; however, the 0.9 mm–800 mm/s and 1.5 mm–8 mm/s injury groups displayed a trend toward increased deficit. This trend led to further investigation of forelimb function and displayed noticeable reduction of forelimb score ( $p = 0.003743$ ) between these groups (Fig. 3B).

Correlation analysis of the behavioral open-field scores showed significant ( $p < 0.05$ ) relationship with both the speed and depth of impact. Impact depth displayed considerably higher correlation with postinjury forelimb ( $R = -0.70$ ), hindlimb ( $R = -0.66$ ), total scores ( $R = -0.66$ ), with increasing depth resulting in lower overall scores. Impact speed showed correlation with both total ( $R = -0.38$ ) and hindlimb score ( $R = -0.33$ ), but not forelimb score.

**Tissue sparing**

The percentage of tissue sparing at the epicenter and each 1-mm increment rostral and caudal was analyzed using a standard ratio of the total area of intact GM or WM versus total tissue. Sections of damaged tissue were stained with LFB to detect gross tissue sparing (Fig. 4A). A multi-factorial ANOVA revealed significant main effects of impact depth ( $p < 0.01$ ), impact speed ( $p = 0.012$ ), and a significant interaction between depth and speed ( $p = 0.0055$ ) at the epicenter of injury on WM sparing (Fig. 4B). GM sparing only displayed significant effects of impact depth ( $p < 0.01$ ; Fig. 4C). The 1.5-mm impact depth injury groups showed less WM tissue

TABLE 2. KINETIC IMPACT DATA AFTER INJURY

Group	Impact depth (mm)	Impact speed (mm/s)	Force (N)	Energy applied (mJ)
1	0.896 (0.002)	8.797 (1.003)	0.637 (0.106)	0.250 (0.038)
2	0.880 (0.003)	83.800 (1.112)	0.794 (0.105)	0.356 (0.050)
3	0.888 (0.003)	838.272 (2.921)	0.903 (0.199)	0.506 (0.088)
4	1.471 (0.032)	8.263 (0.928)	1.201 (0.112)	0.711 (0.074)
5	1.459 (0.006)	83.868 (1.396)	1.770 (0.232)	1.187 (0.180)
6	1.461 (0.006)	840.555 (1.696)	2.134 (0.266)	1.775 (0.209)
7	N/A	N/A	N/A	N/A

Values shown are mean ( $\pm$  standard deviation).  
N/A, not available.

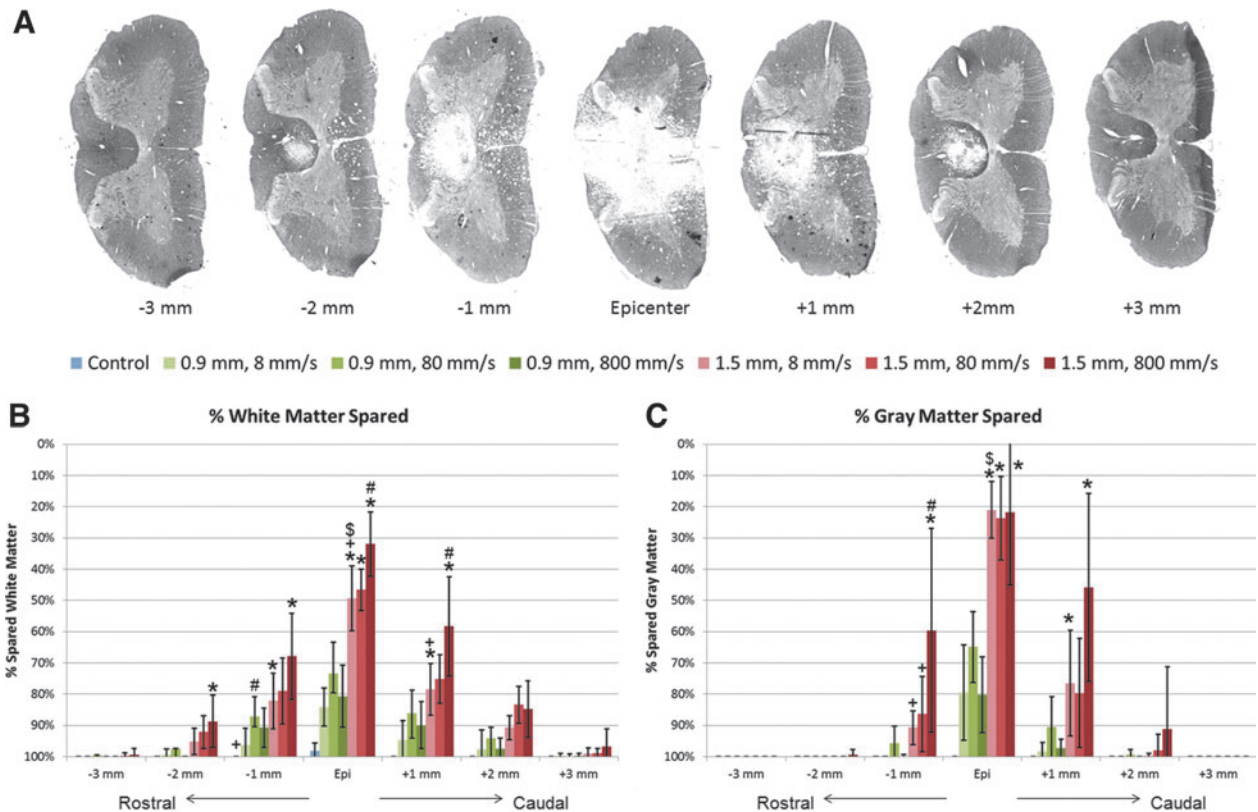


**FIG. 4.** (A) Luxol fast blue stained spinal cord tissue at 1 mm increments. The area percentages of (B) white matter spared and (C) gray matter spared were calculated as the ratio of intact tissue versus total tissue. \* $p < 0.05$ , compared to the 0.9-mm impact depth injury at the same impact velocity; # $p < 0.05$ , compared to the 8-mm/s impact velocity at the same impact depth; + $p < 0.05$ , compared to the 800-mm/s impact velocity at the same impact depth; \$ $p < 0.05$  between the 1.5 mm–8 mm/s and 0.9 mm–800 mm/s groups (similar impact energy range). Data shown are group means  $\pm$  standard deviation. Color image is available online at [www.liebertpub.com/neu](http://www.liebertpub.com/neu)

sparing than the control animals up to  $\pm 2$  mm from the injury epicenter; the 0.9-mm impact depth displayed less tissue sparing up to  $\pm 1$  mm from the epicenter.

#### Nerve fiber damage

The percentage of damaged and demyelinated nerve fibers at each 1-mm interval from the injury epicenter, in both the ventral and lateral regions of the spinal cord, were analyzed using the ratio of damaged to total nerve fibers in the tissue. For the ventral region of the spinal cord, a multi-factorial ANOVA revealed the significant main effects of impact depth ( $p < 0.01$ ), impact speed ( $p < 0.01$ ), and a significant interaction between depth and speed ( $p = 0.0077$ ) at the epicenter. These factors remained significant at each interval from the epicenter to 3 mm rostral and caudal, affecting the percentage of damaged and demyelinated nerve fibers. Results plotted in Figure 5 show that, at the epicenter of injury, increased impact depth, regardless of impact speed, resulted in a significant increase in the percentage of damaged nerve fibers ( $p < 0.01$ ). Increased impact speed was only a significant effect at the 1.5-mm impact depth ( $p < 0.01$ ) or when increased from 8 to 800 mm/s at the 0.9-mm impact depth ( $p < 0.01$ ). The 1.5 mm–8 mm/s group also showed an increase in percentage of damaged nerve fibers over the 0.9 mm–800 mm/s group ( $p < 0.01$ ) up to  $\pm 2$  mm from epicenter, although the applied energy was within a similar range. Impact speed displayed a diminishing effect on the amount of damaged nerve fibers further from the injury epicenter than impact depth in the ventral region.

In the lateral region of the spinal cord, a multi-factorial ANOVA revealed the significant main effects of impact depth ( $p < 0.01$ ), impact speed ( $p < 0.01$ ), and depth\*speed ( $p < 0.01$ ) at the injury epicenter. The interactive effect of depth\*speed disappeared at  $\pm 1$  mm, and impact speed had no significant effect on the percentage of damaged nerve fibers beyond  $\pm 2$  mm. At the injury epicenter, the percentage of damaged nerve fibers in the lateral region of the spinal cord was significantly increased by both increasing impact speed ( $p < 0.05$ ) and impact depth ( $p < 0.001$ ; Fig. 6). Comparison between the 1.5 mm–8 mm/s and 0.9 mm–800 mm/s groups showed no statistical increase of damaged nerve fibers with a similar range of impact energy applied to the cord. At  $\pm 1$  mm from the epicenter, the effect of increased impact depth on the percentage of demyelinated axons disappeared. Similarly, the effect of increased impact speed was reduced and only saw significance between the 1.5-mm group from 8 to 80 mm/s at  $-1$  mm ( $p = 0.047$ ). In contrast to the results observed in the ventral region, neither increased impact depth nor impact speed significantly increased the percentage of damaged nerve fibers beyond  $\pm 1$  mm in the lateral WM.

#### Correlations with maximum principal strain

Corresponding experimental displacement and force profiles were compared with the FEA results using similar simulation corridors of  $\pm 2$  SDs used by Russell and colleagues in the validation data (Fig. 7).<sup>28</sup> Simulation displacements displayed a similar trace and peak value as the data recorded experimentally. The simulated contact forces also showed similar trace patterns as the

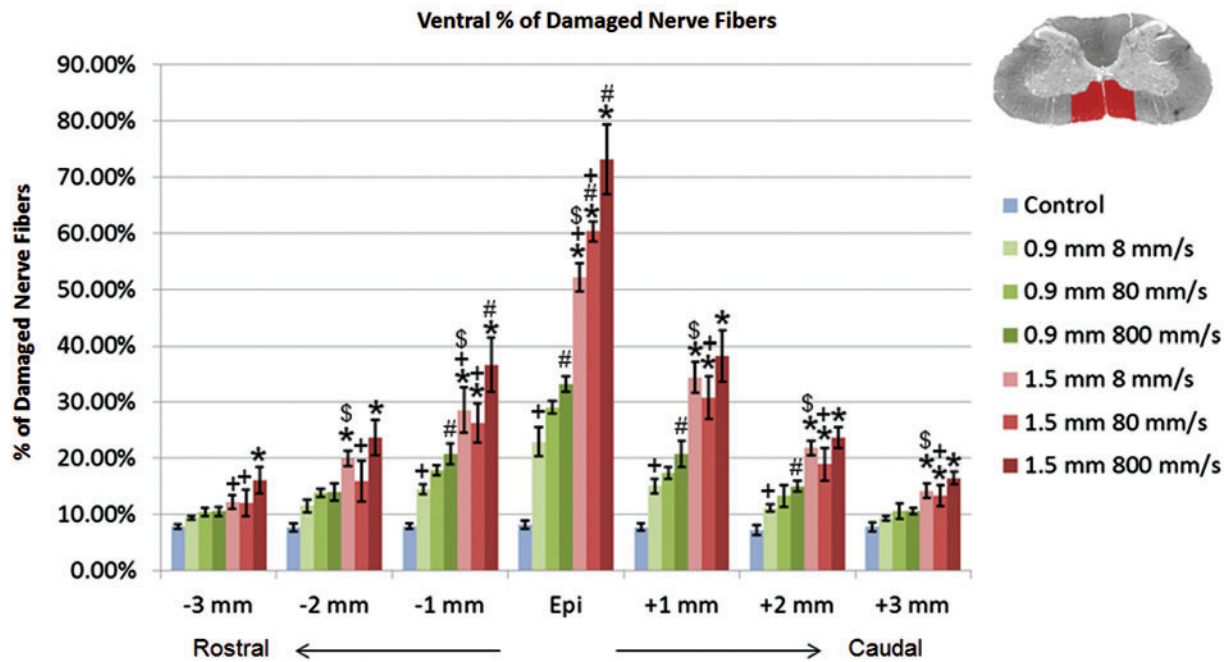


**FIG. 5.** Percentage of damaged nerve fibers in the ventral region of the spinal cord tissue. \* $p < 0.01$ , compared to the 0.9-mm impact depth injury at the same impact velocity; # $p < 0.05$ , compared to the 8-mm/s impact velocity at the same impact depth; + $p < 0.05$ , compared to the 800-mm/s impact velocity at the same impact depth; \$ $p < 0.05$  between the 1.5-mm–8 mm/s and 0.9-mm–800 mm/s groups (similar impact energy range). Data shown are group means  $\pm$  standard deviation. Color image is available online at [www.liebertpub.com/neu](http://www.liebertpub.com/neu)

experimental data, but had lower peak values. There was also a slight lag (between 1 and 1.5 ms) in the simulated force data, compared to the experimental results recorded by the UBC multi-mechanism injury system. Contusion injuries showed a uniform distribution of strain, the ratio of compression or elongation of the tissue to its

original shape, around the epicenter of injury spreading out as far as 3 mm both rostral and caudal. The cross-sectional distribution of strain also shows a mirrored strain pattern around the centerline.

All WM regions in the model (ventromedial, ventrolateral, left lateral, right lateral, and dorsal) were collected and averaged, which

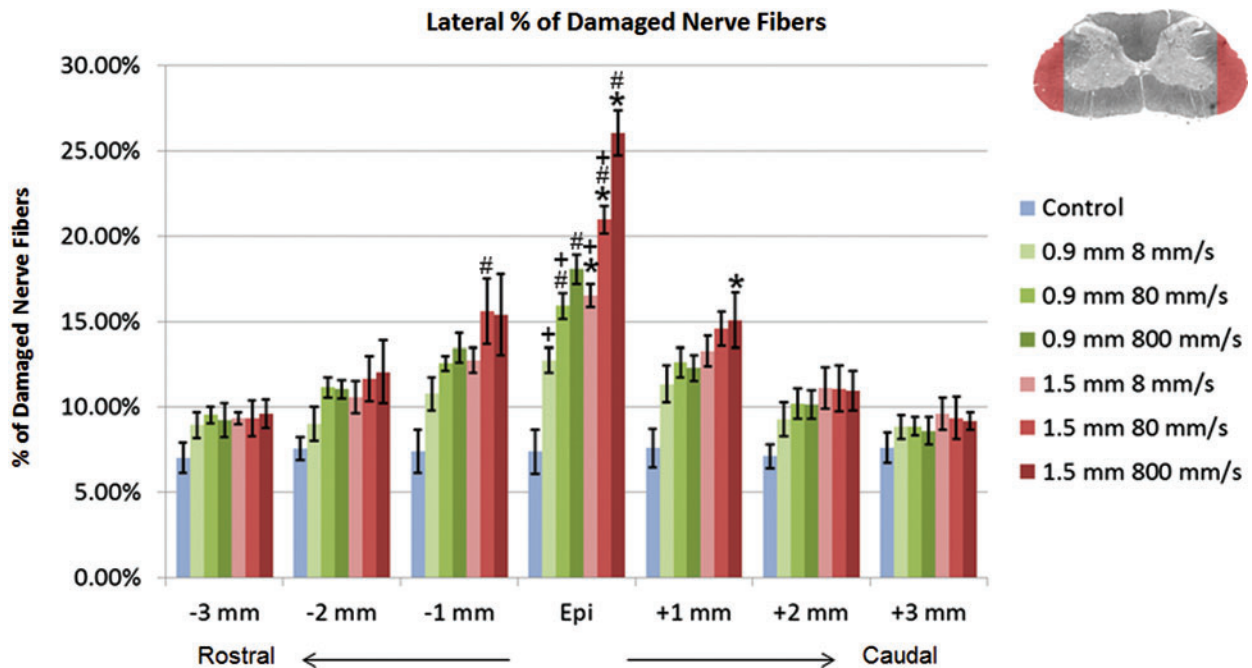


**FIG. 6.** Percentage of damaged nerve fibers in the lateral region of the spinal cord tissue. \* $p < 0.01$ , compared to the 0.9-mm impact depth injury at the same impact velocity; # $p < 0.05$ , compared to the 8-mm/s impact velocity at the same impact depth; + $p < 0.05$ , compared to the 800-mm/s impact velocity at the same impact depth. Data shown are group means  $\pm$  standard deviation. Color image is available online at [www.liebertpub.com/neu](http://www.liebertpub.com/neu)

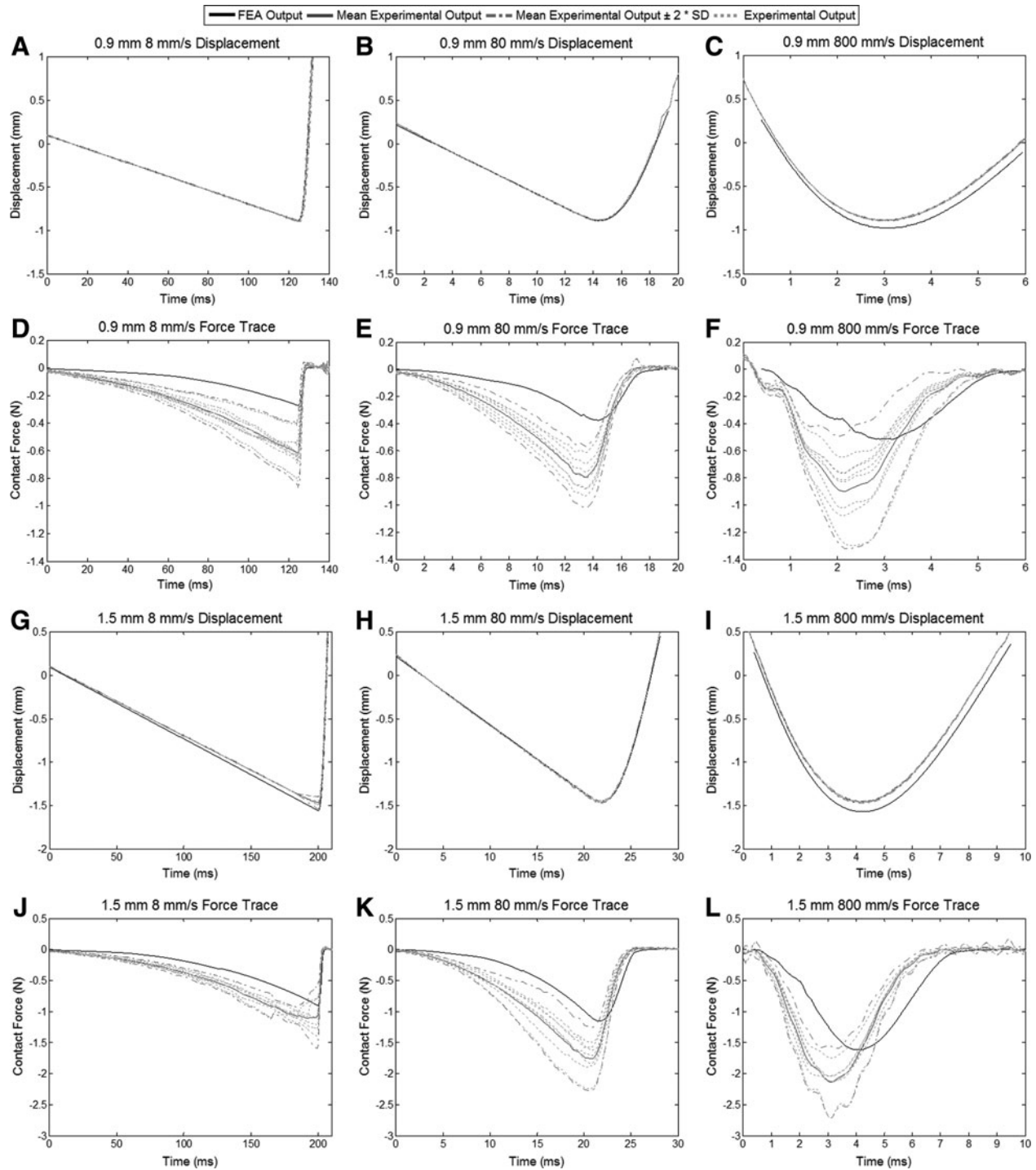


**FIG. 7.** Experimental displacements and contact forces with the dura plotted alongside the simulated displacement and force traces. (A, B, C, G, H, and I) Simulated impactor displacement for all injury groups matches closely with the mean experimental displacement. The 800-mm/s impact velocities show a slight deviation away from the experimental displacement, but follow the same pattern. (D, E, F, J, K, and L) Simulated contusion forces follow the same patterns as recorded by the load cell experimentally. Peak forces are lower in the finite element model and lag behind the experimental data by approximately 1.0–1.5 ms in all injury groups. FEA, finite element analysis; SD, standard deviation.

showed significant ( $p < 0.001$ ) correlation with WM sparing ( $R^2 = 0.90$ ; Fig. 8A), pooled from all experimental injury groups (Fig. 9). Less tissue spared with increased strain in the ventral GM also showed significant ( $p < 0.001$ ) correlation ( $R^2 = 0.76$ ; Fig. 8B). In addition to the correlations with WM and GM sparing, a measure

of the whole GM/WM damage, were the strong correlations with the region-specific percentage of axons damaged or demyelinated. Increased strain was strongly tied to an increased percentage of axons becoming damaged in the ventral ( $R^2 = 0.86$ ; Fig. 8C) and lateral ( $R^2 = 0.74$ ; Fig. 8D) regions of the spinal cord. Table 3

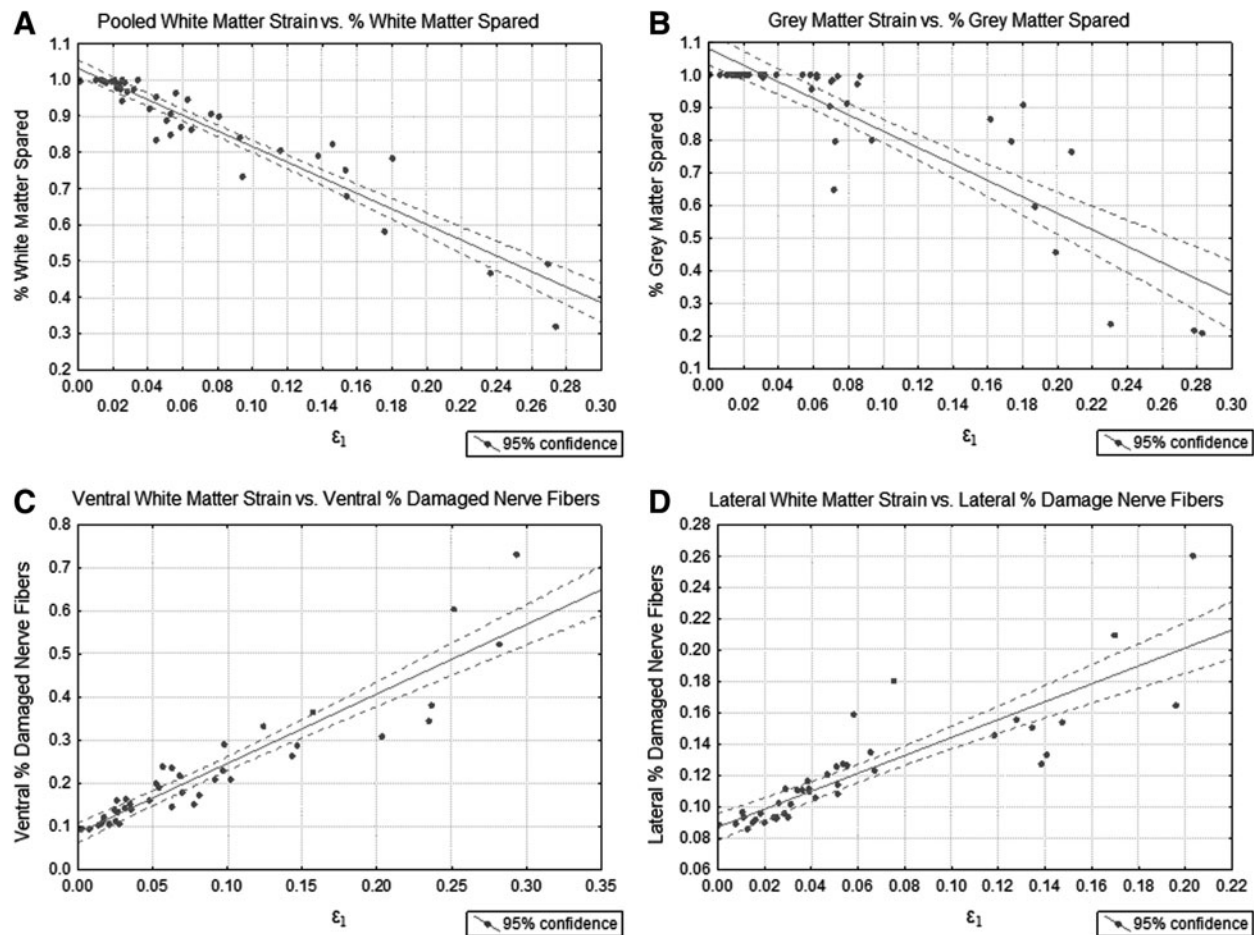


**FIG. 8.** Correlations of maximum principal strain with (A) percent spared white and (B) percent spared gray matter. Maximum principal strain correlations with percent of damaged or demyelinated nerve fibers are shown in the (C) ventral region and (D) lateral region of the spinal cord.

provides a summary of all correlation coefficients between the mechanical impact factors and histological analysis with maximum principal strain.

Comparison of the relationship between the open-field behavioral analysis and finite element model (FEM) maximum principal strain showed strong nonparametric correlations. For the pooled WM strain, significant ( $p < 0.05$ ) correlations were shown with postinjury total score ( $R = -0.94$ ), forelimb score ( $R = -0.81$ ), and hindlimb score ( $R = -0.94$ ), with lower scores with increasing strain (Table 4). The GM strain displayed significant ( $p < 0.05$ ) correlations with both postinjury total score ( $R = -0.94$ ) and forelimb score ( $R = -0.84$ ). No correlation existed between the GM strain and postinjury hindlimb score.

## Discussion

### *Effects of contusion impact depth and speed on secondary injury*

This study was designed to examine both the individual and interactive effects of a large range of contusion impact velocities and depths in SCI at 7 days postinjury. Much of the existing research has not decoupled the control of these mechanical impact factors independently. This has been a result of the inherent coupling between impact depth and speed in weight drop models, such as the New York University (NYU) impactor, and the lack of

independent control of these variables. Other electromechanical impactors, such as the Infinite Horizons impactor, operate on force-feedback, but cannot alternatively control impact depth and speed as the UBC multi-mechanism injury system can. The effects of these individual parameters have been demonstrated by this research and by others to be important to understanding the biomechanics of contusion SCI.<sup>10,30-32</sup> To our knowledge, this research is the first study to control both impact speed and depth independently within the same experimental matrix, while also intending to apply similar impact energy with different impact factors in a contusion injury. An understanding of the response of the spinal cord to these types of injuries might help eventually identify areas of greater susceptibility or improve targeted treatments clinically.

In the behavioral and histological assessment of the six injury groups, both the increased impact speed and impact depth showed significant increase in damage to the spinal cord. Specifically, the interactive effects between the two impact factors play an important role in tissue sparing and axon demyelination within  $\pm 1$  mm of the injury epicentre. Kim and colleagues found that, in mice, there was no effect of impact speed given a fixed impact depth in contusion injury,<sup>33</sup> which was only observed in this study at the low impact depth of 0.9 mm. Interactive effects between these two parameters are shown to be important here; the depth of injury in the previously mentioned study may not have been great enough to elicit a significant difference between increased impact velocities.

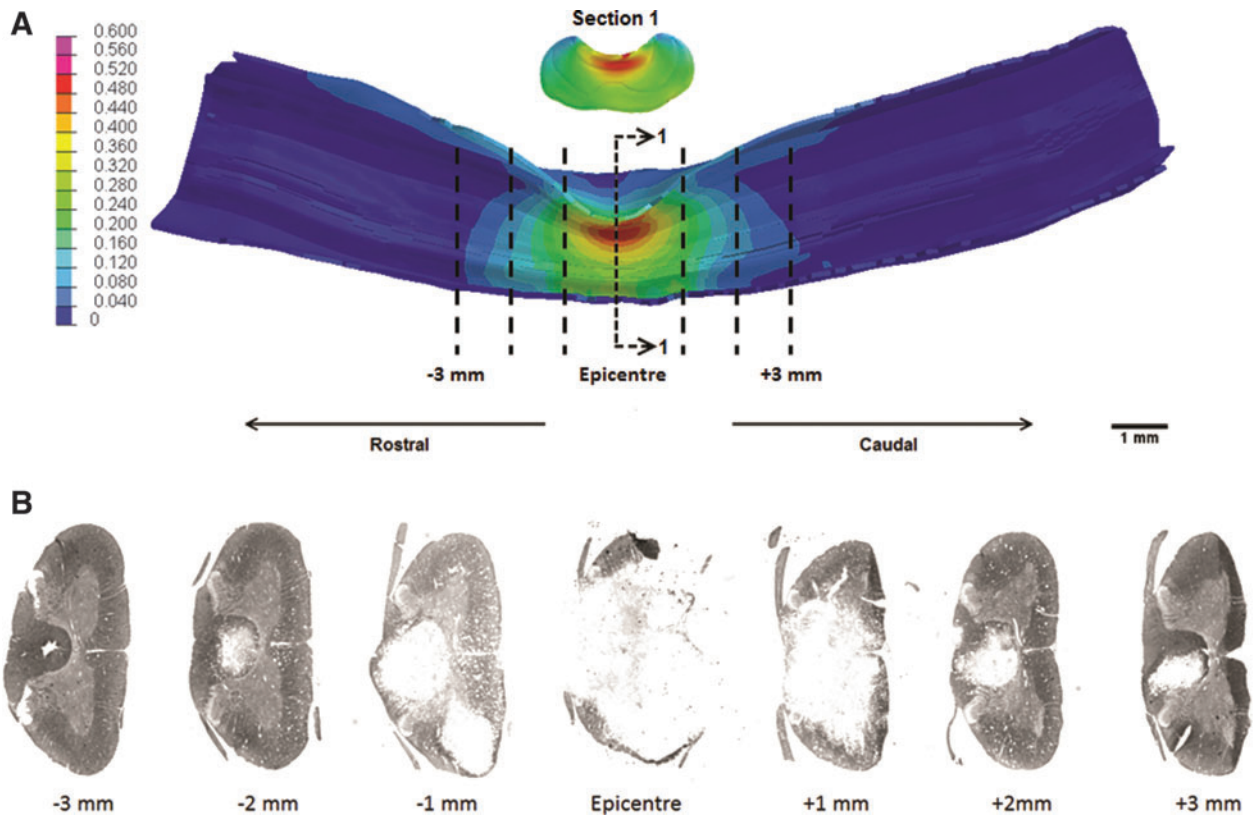


**FIG. 9.** (A) Computational peak principal strain patterns in the 1.5 mm–800 mm/sec injury group and the (B) corresponding myelin-based protein stain cross-sections used to quantify tissue sparing. Color image is available online at [www.liebertpub.com/neu](http://www.liebertpub.com/neu)

The idea of this interaction between mechanical measurements of soft tissue injury was first studied by Viano and Lau<sup>34</sup> and extended to the spinal cord by Kearney in 1988.<sup>8</sup> It was shown that, at low impact speed, the impact depth acts as the primary mechanical effect on the injury severity of contusion SCI, but with increasing speed, the viscous response of the cord becomes more important.

Here, similar results are observed with impact depth appearing to be a consistent predictor of injury severity, while speed becomes more important only once a threshold depth has been achieved. However, fundamental mechanics equations show that adding more energy that can do work on an object should result in higher displacement, or strain in the case of spinal cord injury, as a result. This increased strain has been linked to increasing functional deficit in SCI.<sup>15,28,35,36</sup> The importance of the viscous response here can be identified by the results of the energy measurements of each injury group, where increased impact depth results in a significant increase in the energy applied to the cord, whereas the increased

speed creates a similar increase in applied energy only at the 1.5-mm impact depth.

There appears to be a point in the combination between impact speed and depth where relative increases in either will significantly increase the energy applied to the spinal cord and therefore the severity of injury. Below this threshold, somewhere between the 0.9 mm–800 mm/s and 1.5 mm–8 mm/s injury combination in these animals, the viscous response of the cord appears to be less important and severity is defined by the depth of the impact.

The tissue mechanics of the spinal cord structure is not yet fully understood; however, the results from this study identify both a viscous and elastic component, as displayed by many soft biological tissues. At low impact depths, the mechanical response of the cord appears to be similar over a relatively wide range of strain

**TABLE 3.** CORRELATION COEFFICIENTS FOR MAXIMUM PRINCIPAL STRAIN WITH LFB/MBP HISTOLOGY

	p value	Correlation coefficient (R <sup>2</sup> )
% white matter spared	9.87E-22	0.90
% gray matter spared	7.29E-14	0.76
Ventral % damaged nerve fibers	5.78E-19	0.86
Lateral % damaged nerve fibers	3.66E-13	0.74

LFB, Luxol fast blue; MBP, myelin-based protein.

**TABLE 4.** CORRELATION COEFFICIENTS FOR MAXIMUM PRINCIPAL STRAIN WITH OPEN-FIELD BEHAVIORAL SCORES

	Pooled white matter strain		Gray matter strain	
	p value	Spearman's rank correlation coefficient (r <sub>s</sub> )	p value	Spearman's rank correlation coefficient (r <sub>s</sub> )
7 days postinjury				
Total score	0.005	−0.94	0.005	−0.94
Forelimb score	0.049	−0.81	0.036	−0.84
Hindlimb score	0.005	−0.94	0.072	NS

NS, not significant.

rates, displaying a primarily elastic response. This response may help describe spinal cord tissue mechanics, but would require a more in-depth study of impact parameters for increased confidence.

#### *Behavioral deficit*

This study compared the outcome of a contusion SCI through behavioral analysis, demyelination of axons in the spinal cord, tissue sparing, and principal strain at a time point postinjury where the earliest stages of secondary injury effects could be observed.<sup>37,38</sup> Open-field behavior analysis showed statistically significant results of the interactive effects between impact velocity and depth and hinted at the energy effects of impact. Only groups that received injuries at 1.5 mm showed significant reduction in score from their baseline measurements, whereas changes in velocity had no effect. The 0.9 mm–800 mm/s and 1.5 mm–8 mm/s injury groups displayed trends in total score and forelimb function, suggesting that, although a similar energy range was applied to the cord, there were differences in the behavioral deficit measurements. A likely explanation for this observation is the greater strain, observed in the 1.5-mm impact, experienced by the nerve fibers in the ventral vestibulospinal and reticulospinal tracts, causing demyelination and affecting movement-related activities. Though trends were observed in the data suggesting potential differences in behavioral deficit with similar impact energy, a more sensitive behavioral test may be needed to tease out these differences between these groups.

#### *Tissue sparing and axonal damage*

In the current study, spinal cord tissue analysis supplemented the behavioral observations to provide additional explanation for deficits or lack thereof. Holistic WM and GM damage observed with the LFB stain showed distinct differences in the contributions to tissue damage from increasing impact velocity or depth. Although impact depth, velocity, and the interaction between the two showed significant effects on the amount of WM spared at the epicenter, the interactive and velocity effects very quickly dropped off further away from the epicenter. Given the decreasing strain in the sections further from the epicenter, it should be expected that impact velocity becomes less important as we are moving further from the interaction effect threshold. In the GM, it was immediately evident that impact depth was the only factor that suggested influence on the amount of tissue spared in that region.

In the WM, the demyelination of axons in the ventral and lateral regions causes the impairment of signal transmission in the central nervous system.<sup>19–21,39</sup> Demyelination of the axons in the spinal cord has been considered a major contributor to functional loss after SCI resulting from the impaired signal conduction and action potential propagation.<sup>40</sup> This study suggests that increased impact velocity and depth result in significant nerve fiber pathology, including widespread damage to the nerve fibers after contusion injuries. Similarly, as shown by the behavioral and LFB analysis, the increase of impact depth consistently increased the amount of demyelination of axons in the ventral region of the spinal cord. Change in impact speed was important in the 1.5-mm impact depth groups and when increased from 8 to 800 mm/s in the 0.9-mm impact depth groups.

It is also important to note that the residual WM at the epicenter, as revealed by LFB, contained a high percentage of nerve fiber pathology. Hence, LFB staining clearly underestimated the actual WM damage. This is most likely a result of the fact that this stain also binds to damaged nerve fibers as well as myelin debris notorious for lingering around for many weeks after injury.

#### *Contusion finite element analysis*

In addition to observing the effects of mechanical factors on injury severity in SCI, the examination of the mechanical response of the spinal cord, such as impact strain, was displayed as a predictor for biological damage and behavioral deficit. Overall, the response of the FEM demonstrated its biofidelity, simulating contusion injuries over a range of impact velocities and depths. No correlation existed between the GM strain and postinjury hindlimb score. This may be explained by the fact that cervical spinal cord injuries result mainly in forelimb deficit and that the functional responsibility of the GM tissue is to control the signals at a specific vertebral level only. Contact forces, although slightly lower than shown experimentally, were within realistic values with nearly identical displacement and velocity profiles. The strain patterns and range of maximum principal strain values calculated by this model displayed similarity to both the cervical cord results observed by Russell and colleagues<sup>28</sup> as well as thoracic cord model developed by Maikos and colleagues.<sup>35</sup>

Results from this work show very strong correlations between maximum principal strain and spinal cord tissue damage, supporting previous research strengthening the validity and potential utility of this FEM.<sup>15,16,35</sup> These correlations did not specifically identify any tolerance threshold of tissue damage; however, the strain was only greater than the 0.14 tolerance threshold determined by Bain and colleagues for the 1.5-mm impact depth groups within  $\pm 1$  mm of the injury epicenter, where the correlations to axonal damage were the strongest.<sup>15</sup>

#### *Limitations*

Several limitations of the current work leave the possibility for improvement in the future. A common limitation of displacement-controlled contusion impact models is the requirement to find a common initial position to define the datum. This study, along with others, used a small contact force of 0.03 N as the starting point for all impacts.<sup>25,26,41</sup> The measured force, at the resolution provided by the load cell, did fluctuate after reaching the initial 0.03-N reading as a result of the viscoelasticity of the cord, response of the dura, and the presence of the CSF. Though variations in the forces were small, altering the datum could result in a larger or smaller absolute cord compression depth than in other contusions of the same injury group. Without real-time and simple imaging techniques to allow a view of the spinal cord and impactor position, force control to the first measurement of 0.03 N was used to minimize variation.

Contusion injuries in this study were mid-line C5/C6 cervical spine impacts, and though both the behavioral and histological results agree with this, mediolateral and rostrocaudal alignment were done by hand. Markings on the clamp, in addition to consultation with the surgeon, identified the centerline rostrocaudally and mediolaterally on the spinal cord while adjusting impactor position. To ensure that any variation in the alignment was distributed evenly among all groups, a single researcher performed all set-up and alignment procedures.

The contusion injuries applied in this work impacted the dorsal side of the spinal cord. In humans, SCIs occur on the ventral, or anterior, side of the cord as a result of a bone fragment fracture impinging the cord. Presently, ventral contusion injuries have not been modeled given the difficulty of accessing the spinal cord through the anterior side of the animal without potentially damaging other internal organs. The strain patterns and resulting tissue damage presented in this study are a representation of dorsal impacts only.

Finally, the computational model used in the current study was a modification of the rat cervical spine developed by Russell and colleagues and inherently retains the same limitations, primarily in the definition of the material properties, given the lack of consensus on the differences in material properties for the GM and WM independently.<sup>28,35</sup> Material properties were initially determined by a hyperviscoelastic model and adjusted to comply with experimental behavior. This material model could be improved with further validation with whole-cord behavior to fully simulate the response of the spinal cord. Particularly, the hyper- and viscoelastic constants were developed using data based on the experimental strain of rat spinal cord tissue of only up to 5%, and the cord was assumed to be isotropic and homogeneous.<sup>28,32</sup> This may affect the absolute value of the predicted strain; however, given that the material homogeneity is consistent in all computational models, the effect on the relative strain distributions was consistent. Although these values provided a concrete starting point for the development of the material model, more-detailed characterization of the rat spinal cord experimentally, along with more-complex, fully nonlinear, viscoelastic models may be necessary to simulate a more accurate response. This model also did not include structural failure for the GM or WM, which may create different strain patterns in the tissue.

## Conclusion

In conclusion, we found that, in a rodent model of contusion SCI, impact depth is always an important and determining factor in injury severity. Impact speed displayed an interactive role with impact depth, becoming more important in determining injury severity beyond a depth threshold. Although the existence of an interaction threshold was shown by this work, no specific values were determined and may require a larger experimental matrix or regression model to specifically identify. The current work also extends the research identifying significant correlation between maximum principal strain and neurological tissue damage. This study has demonstrated that contusion injuries at a deeper impact show a more speed-sensitive response to injury than a shallow one. This improves our general understanding of SCI biomechanics. It may also help identify potential regions of the spinal cord for targeted therapies based on predicted injury patterns caused at different speeds and depths.

## Acknowledgments

The authors are thankful to the Natural Sciences and Engineering Research Council of Canada (NSERC) for financial support. P.A. is supported by a Frederick Banting and Charles Best Canadian Graduate Scholarship-Doctoral Award.

## Author Disclosure Statement

No competing financial interests exist.

## References

- Pickett, G.E., Campos-Benitez, M., Keller, J.L., and Duggal, N. (2006). Epidemiology of traumatic spinal cord injury in Canada. *Spine* 31, 799–805.
- Sekhon, L.H., and Fehlings, M.G. (2001). Epidemiology, demographics, and pathophysiology of acute spinal cord injury. *Spine* 26, Suppl. 24, S2–S12.
- National Spinal Cord Injury Statistical Center at the University of Alabama at Birmingham. (2012). Spinal cord injury facts and figures at a glance. Technical report, 2012. University of Alabama: Birmingham, AL.
- Noonan, V.K., Fingas, M., Farry, A., Baxter, D., Singh, A., Fehlings, M.G., and Dvorak, M.F. (2012). Incidence and prevalence of spinal cord injury in Canada: a national perspective. *Neuroepidemiology* 38, 219–226.
- Cao, Y., Chen, Y., and DeVivo, M. (2011). Lifetime direct costs after spinal cord injury. *Topics Spinal Cord Inj. Rehabil.* 16, 10–16.
- Bresnahan, J.C., Beattie, M.S., Todd, F.D., III, and Noyes, D.H. (1987). A behavioral and anatomical analysis of spinal cord injury produced by a feedback-controlled impaction device. *Exp. Neurol.* 95, 548–570.
- Gruner, J.A. (1992). A monitored contusion model of spinal cord injury in the rat. *J. Neurotrauma* 9, 123–126; discussion, 126–128.
- Kearney, P.A., Ridella, S.A., Viano, D.C., and Anderson, T.E. (1988). Interaction of contact velocity and cord compression in determining the severity of spinal cord injury. *J. Neurotrauma* 5, 187–208.
- Sparrey, C.J., Choo, A.M., Liu, J., Tetzlaff, W., and Oxlund, T.R. (2008). The distribution of tissue damage in the spinal cord is influenced by the contusion velocity. *Spine* 33, E812–E819.
- Maikos, J.T., and Shreiber, D.I. (2007). Immediate damage to the blood-spinal cord barrier due to mechanical trauma. *J. Neurotrauma* 24, 492–507.
- Bresnahan, J.C., Beattie, M.S., Stokes, B.T., and Conway, K.M. (1991). Three-dimensional computer-assisted analysis of graded contusion lesions in the spinal cord of the rat. *J. Neurotrauma* 8, 91–101.
- Behrmann, D.L., Bresnahan, J.C., Beattie, M.S., and Shah, B.R. (1992). Spinal cord injury produced by consistent mechanical displacement of the cord in rats: behavioral and histologic analysis. *J. Neurotrauma* 9, 197–217.
- Noyes, D.H. (1987). Correlation between parameters of spinal cord impact and resultant injury. *Exp. Neurol.* 95, 535–547.
- Pearse, D.D., Lo, T.P., Jr., Cho, K.S., Lynch, M.P., Garg, M.S., Marcillo, A.E., Sanchez, A.R., Cruz, Y., and Dietrich, W.D. (2005). Histopathological and behavioral characterization of a novel cervical spinal cord displacement contusion injury in the rat. *J. Neurotrauma* 22, 680–702.
- Bain, A.C., and Meaney, D.F. (2000). Tissue-level thresholds for axonal damage in an experimental model of central nervous system white matter injury. *J. Biomech. Eng.* 122, 615–622.
- Bain, A.C., Raghupathi, R., and Meaney, D.F. (2001). Dynamic stretch correlates to both morphological abnormalities and electrophysiological impairment in a model of traumatic axonal injury. *J. Neurotrauma* 18, 499–511.
- Norenberg, M.D., Smith, J., and Marcillo, A. (2004). The pathology of human spinal cord injury: defining the problems. *J. Neurotrauma* 21, 429–440.
- Blight, A.R. (1985). Delayed demyelination and macrophage invasion: a candidate for secondary cell damage in spinal cord injury. *Cent. Nerv. Syst. Trauma* 2, 299–315.
- Goto, T., and Hoshino, Y. (2001). Electrophysiological, histological, and behavioral studies in a cat with acute compression of the spinal cord. *J. Orthop. Sci.* 6, 59–67.
- Waxman, S.G. (1989). Demyelination in spinal cord injury. *J. Neurol. Sci.* 91, 1–14.
- Totoiu, M.O., and Keirstead, H.S. (2005). Spinal cord injury is accompanied by chronic progressive demyelination. *J. Comp. Neurol.* 486, 373–383.
- Siegenthaler, M.M., Tu, M.K., and Keirstead, H.S. (2007). The extent of myelin pathology differs following contusion and transection spinal cord injury. *J. Neurotrauma* 24, 1631–1646.
- Lau, N.S., Gorrie, C.A., Chia, J.Y., Bilston, L.E., and Clarke, E.C. (2013). Severity of spinal cord injury in adult and infant rats after vertebral dislocation depends upon displacement but not speed. *J. Neurotrauma* 30, 1361–1373.
- Martinez, M., Brezun, J.M., Bonnier, L., and Xerri, C. (2009). A new rating scale for open-field evaluation of behavioral recovery after cervical spinal cord injury in rats. *J. Neurotrauma* 26, 1043–1053.
- Choo, A.M., Liu, J., Lam, C.K., Dvorak, M., Tetzlaff, W., and Oxlund, T.R. (2007). Contusion, dislocation, and distraction: primary hemorrhage and membrane permeability in distinct mechanisms of spinal cord injury. *J. Neurosurg. Spine* 6, 255–266.
- Stokes, B.T., Noyes, D.H., and Behrmann, D.L. (1992). An electromechanical spinal injury technique with dynamic sensitivity. *J. Neurotrauma* 9, 187–195.
- Gale, K., Kerasidis, H., and Wrathall, J.R. (1985). Spinal cord contusion in the rat: behavioral analysis of functional neurologic impairment. *Exp. Neurol.* 88, 123–134.

28. Russell, C.M., Choo, A.M., Tetzlaff, W., Chung, T.E., and Oxland, T.R. (2012). Maximum principal strain correlates with spinal cord tissue damage in contusion and dislocation injuries in the rat cervical spine. *J. Neurotrauma* 29, 1574–1585.
29. Choo, A.M., Liu, J., Dvorak, M., Tetzlaff, W., and Oxland, T.R. (2008). Secondary pathology following contusion, dislocation, and distraction spinal cord injuries. *Exp. Neurol.* 212, 490–506.
30. Bilston, L.E., and Thibault, L.E. (1996). The mechanical properties of the human cervical spinal cord in vitro. *Ann. Biomed. Eng.* 24, 67–74.
31. Cheng, S., Clarke, E.C., and Bilston, L.E. (2009). The effects of preconditioning strain on measured tissue properties. *J. Biomech.* 42, 1360–1362.
32. Fiford, R.J., and Bilston, L.E. (2005). The mechanical properties of rat spinal cord in vitro. *J. Biomech.* 38, 1509–1515.
33. Kim, J.H., Tu, T.W., Bayly, P.V., and Song, S.K. (2009). Impact speed does not determine severity of spinal cord injury in mice with fixed impact displacement. *J. Neurotrauma* 26, 1395–1404.
34. Viano, D.C., and Lau, I.V. (1988). A viscous tolerance criterion for soft tissue injury assessment. *J. Biomech.* 21, 387–399.
35. Maikos, J.T., Qian, Z., Metaxas, D., and Shreiber, D.I. (2008). Finite element analysis of spinal cord injury in the rat. *J. Neurotrauma* 25, 795–816.
36. Zhu, Q., Prange, M., and Margulies, S. (2006). Predicting unconsciousness from a pediatric brain injury threshold. *Dev. Neurosci.* 28, 388–395.
37. Liu, X.Z., Xu, X.M., Hu, R., Du, C., Zhang, S.X., McDonald, J.W., Dong, H.X., Wu, Y.J., Fan, G.S., Jacquin, M.F., Hsu, C.Y., and Choi, D.W. (1997). Neuronal and glial apoptosis after traumatic spinal cord injury. *J. Neurosci.* 17, 5395–5406.
38. Shuman, S.L., Bresnahan, J.C., and Beattie, M.S. (1997). Apoptosis of microglia and oligodendrocytes after spinal cord contusion in rats. *J. Neurosci. Res.* 50, 798–808.
39. McTigue, D.M., Horner, P.J., Stokes, B.T., and Gage, F.H. (1998). Neurotrophin-3 and brain-derived neurotrophic factor induce oligodendrocyte proliferation and myelination of regenerating axons in the contused adult rat spinal cord. *J. Neurosci.* 18, 5354–5365.
40. Nashmi, R., and Fehlings, M.G. (2001). Changes in axonal physiology and morphology after chronic compressive injury of the rat thoracic spinal cord. *Neuroscience* 104, 235–251.
41. Scheff, S.W., Rabchevsky, A.G., Fugaccia, I., Main, J.A., and Lump, J.E., Jr. (2003). Experimental modeling of spinal cord injury: characterization of a force-defined injury device. *J. Neurotrauma* 20, 179–193.

Address correspondence to:

*Thomas R. Oxland, PhD*

*ICORD*

*Blusson Spinal Cord Center*

*818 West 10th Avenue*

*5th Floor*

*Vancouver, British Columbia, Canada V5Z 1M9*

*E-mail: toxland@icord.org*